Fatigue Characteristics of PZT Thin Films Deposited by ECR-PECVD

Su-Ock Chung and Won-Jong Lee[a]

Department of Materials Science and Engineering, KAIST,
Guseong-dong, Yuseong-gu, Daejeon 305-701, Korea

[a]E-mail : wjlee@kaist.ac.kr

Fatigue characteristics of lead zirconate titanate (PZT) films deposited by electron cyclotron resonance plasma enhanced chemical vapor deposition (ECR-PECVD) were investigated. The fatigue characteristics were investigated with respect to PZT film thickness, domain structure, fatigue pulse height, temperature, electrode materials and electrode configurations. The used top and bottom electrode materials were Pt and RuO_2. In the fatigue characteristics with fatigue pulse height and PZT film thickness, the fatigue rates are independent of the applied fatigue pulse height at the electric field regions to saturate the P-E hysteresis and polarization $(P^*, P^\wedge)$ characteristics. The unipolar and bipolar fatigue characteristics of PZT capacitors with four different electrode configurations ($Pt//Pt$, $Pt//RuO_2$, $RuO_2//Pt$, and $RuO_2//RuO_2$) were also investigated. The polarization-shifts during the unipolar fatigue and the temperature dependence of fatigue rate suggest that the migration of charged defects should not be expected in our CVD-PZT films. It seems that the polarization degradations are attributed to the formation of charged defects only at the Pt/PZT interface during the domain switching. The charged defects pin the domain wall at the vicinity of Pt/PZT interface. When the top and bottom electrode configurations are of asymmetric ($Pt//RuO_2$, $RuO_2//Pt$), the internal fields can be generated by the difference of charged defect densities between top and bottom interfaces.

Keywords : PZT, CVD, Fatigue, Electrode, Charged defect

1. INTRODUCTION

Lead zirconate titanate (PZT) is one of the most promising materials for ferroelectric random access memory (FRAM) capacitor due to its high phase transition temperature (T_c), large remanent polarization, excellent radiation immunity, and relatively low fabrication temperature. The most important issue in the application of PZT film for destructive readout (DRO) – ferroelectric random access memory (FRAM) device is polarization fatigue with periodic pulse. Especially, the PZT capacitor with Pt electrode which provides suitable perovskite nucleation sites exhibit a significant fatigue.

There have been numerous models to explain the fatigue of PZT film[1-6]. Most of fatigue models are associated with the oxygen vacancy ($Vo^{\bullet\bullet}$) or oxygen vacancy – lead vacancy ($Vo^{\bullet\bullet}$-V_{Pb}'') associates inhibiting the domain wall motion. Those models are supported by the fact that fatigue endurance can be greatly improved by using a conductive oxide electrode RuO_2, IrO_2,

$(La_xSr_{1-x})CoO_3$, and $YBa_2Cu_3O_{7-x}$ with a certain degree of $Vo^{\bullet\bullet}$ tolerance for their oxygen stoichiometry. In spite of the numerous reports on the fatigue, the kind and the origin of charged defects contributing the fatigue are not clearly clarified. Since the fatigue characteristics of PZT capacitors can be greatly affected by the fabrication methods of PZT films and so many physical parameters governing the fatigue characteristics, the general model to explain all fatigue phenomena would not be expected.

On the other hand, in order to realize the highly integrated FRAM devices in which the storage capacitor has a complex 3-dimensional structure, the PZT films should be fabricated by CVD method. The micro-structures such as preferred orientation, stress, and defects of CVD-PZT films are different from those of sol-gel derived or sputtered PZT films[7]. Since the fatigue characteristics are closely related to the film properties and microstructure, the CVD-PZT film may exhibit different fatigue characteristics compared to the PZT films fabricated by other deposition methods.

Therefore, the fatigue characteristics of CVD-PZT films must be investigated to confirm the reliable operation of highly integrated FRAM devices. In this study, the fatigue characteristics of CVD-PZT films were investigated with the measuring conditions and the microstructures of PZT films. Additionally, for the PZT capacitors with four different electrode configurations (Pt//Pt, Pt//RuO$_2$, RuO$_2$//Pt, and RuO$_2$//RuO$_2$), the unipolar and bipolar fatigue characteristics were investigated. We also tried to suggest the fatigue origin of CVD-PZT films by organizing these results.

2. EXPERIMENTAL

The electron cyclotron resonance plasma enhanced chemical vapor deposition (ECR-PECVD) system was used for deposition of PZT films. The details on the deposition equipment and the experimental procedures are shown in the previous literature[8,9]. Metal-organic (MO) sources used were lead dipivaloylmethane (Pb (DPM)$_2$, Pb(C$_{11}$H$_{19}$O$_2$)$_2$), zirconium t-butoxide (ZrTB, Zr(OC$_3$H$_7$)$_4$), and titanium iso-propoxide (TiIP, Ti (OC$_3$H$_7$)$_4$). Pt(200 nm)/Ti(30 nm)/SiO$_2$/Si (hereafter Pt substrate) and RuO$_2$(200 nm)/SiO$_2$/Si (hereafter RuO$_2$ substrate) were used as bottom electrodes of PZT capacitors. Pt and Ti films were deposited by rf magnetron sputtering at 400 °C and 200 °C respectively on a wet oxidized (100) Si wafer to fabricate the Pt substrate. RuO$_2$ films were deposited by dc magnetron reactive sputtering at 300 °C on a wet oxidized (100) Si wafer to fabricate the Pt substrate. In order to promote the perovskite nucleation, the Ti-oxide seed layer was formed for 1min prior to PZT film deposition. The deposition conditions of PZT films are summarized in Table 1.

The structural phases of PZT films were characterized with an X-ray diffractometer (XRD). XRD patterns of the PZT films were obtained using the Bragg-Brentano (θ-2θ) method with Cu K$_\alpha$ (λ=1.5402 Å) as a radiation source. Chemical compositions of the PZT films were analyzed by wavelength dispersive spectroscopy (WDS). Actual compositions of the PZT films were evaluated by the WDS correction factor of each element as a function of film thickness[10]. In this study, the Zr/(Zr+Ti) ratios of PZT films were in the range of 0.45~0.55. The film thicknesses and surface morphologies of PZT films were obtained by α-step and scanning electron microscopy (SEM), respectively.

Dot type top electrodes (Pt or RuO$_2$) were constructed to measure the electrical characteristics of the PZT films. Pt dots were deposited using a shadow mask and rf magnetron sputtering at room temperature, 2.2 W/cm^2, and 3 mTorr. RuO$_2$ dots were deposited using dc

Table 1. ECR-PECVD conditions of PZT films.

Bottom Electrode	Pt(200 nm)/Ti(30 nm)/SiO$_2$/Si RuO$_2$(300 nm)/SiO$_2$/Si
Substrate Temp.	450 °C
Sources	
- O$_2$	30 sccm
- Pb(DPM)$_2$	0.20 sccm
- TiIP	0.15 sccm
- ZrTB	0.16 sccm
Carrier Ar	11 sccm
Process Pressure	2 mTorr
Microwave Power	520 watt
Deposition Time	40 min

magnetron sputtering at 300 °C, 2.3 W/cm^2, and 4 mTorr.

The dot areas of Pt and RuO$_2$ were 0.8×10^{-3} cm^2 and 1.2×10^{-3} cm^2, respectively. In order to release the sputtering damage of PZT films at the vicinity of top electrode interface during the top electrode fabrication, the post rapid thermal annealing (RTA) was carried out for 1min at 650 °C in an air ambient. The leakage current characteristics (J-E) of PZT capacitors were measured using a HP 4140 pA meter under the following conditions: pulse voltage of ±3 V, hold time of 30 s, voltage step of 0.1 V, and step-delay time of 1 s. The capacitance characteristics of PZT capacitors were obtained using a HP4192B impedance analyzer. The P-E hysteresis characteristics of PZT capacitors were obtained using an RT66A ferroelectric tester (Radiant Co.) in the virtual ground mode. The switching polarization (P*) and non-switching polarization (P$^{\wedge}$) were also obtained with 2 ms double bipolar pulse in the pulse mode. Polarization fatigue characteristics of PZT capacitors were obtained using an RT66A ferroelectric tester and a HP 8116 pulse function generator that provides bipolar or unipolar square pulses. The temperature dependence of fatigue characteristics was investigated with a TC500 temperature controller in the range of room temperature ~ 80 °C.

The ferroelectric domain structure and orientation were non-destructively analyzed using a domain image mapping of atomic force microscopy (AFM). The equipment for domain image mapping consists of AFM (PSI, CP5 and Autoprobe M5), silicon conducting tip, build-in low pass filter, lock-in amplifier (Standard Research System, SR830), voltage amplifier (Kronhite), and Power PC. Top electrode was not required because the AFM-tip was used as a movable top electrode. In the

AFM-tip/PZT/bottom electrode structure, the small ac signal was applied to induce the local piezo-movement between AFM-tip and bottom electrode. The lock-in amplifier detected the AFM-tip vibration signals by local piezoelectric movement. The polarization orientation of each domain can be determined from the signal.

3. RESULTS AND DISCUSSION

3.1 Electrical and fatigue characteristics with PZT film thickness

The PZT films with different thickness (90 nm, 120 nm, 145 nm, 220 nm) were fabricated on Pt substrate by controlling the deposition time. Ti-oxide seed layers with an average thickness of 4 nm were formed prior to the deposition of PZT films in order to promote the perovskite PZT nucleation. After constructing the Pt top electrode, the electrical properties such as leakage current, capacitance, P-E hysteresis, and fatigue characteristic were investigated with the PZT film thickness.

The chemical compositions, Pb/(Zr+Ti) and Zr/(Zr+Ti) of PZT films were about 0.95 and 0.55 respectively regardless of the film thickness. X-ray diffraction (XRD) patterns showed that all PZT films have only perovskite peaks with different intensity. In the scanning electron microscopy (SEM) images, the PZT films with thicker than 120 nm had large grains with a diameter of about 200 nm, while the 90 nm thick PZT film had relative small grains with a diameter of below 100 nm. The film thickness and the applied bias polarity did not affect the leakage current characteristics of PZT films. In the low electric field range of below 100 kV/cm, their leakage current densities were as low as 10^{-7} A/cm^2.

Figure 1 shows the capacitance characteristics with the different PZT film thickness. In the relationship between zero-biased dielectric constant and film thickness (Fig. 1(a)), the dielectric constant increased with the film thickness. In this study, the Ti-oxide seed layer was used to promote the perovskite PZT nucleation. Additionally, we observed Pb deficient interfacial layer which was formed due to the hard incorporation of Pb elements at the early stage of PZT film deposition[11]. The electrical properties of those interfacial layers are strikingly different from that of the PZT film. In order to investigate the effect of interfacial layer on the electric properties of CVD-PZT films (Fig. 1(b)), the relationship between film thickness (d) and reciprocal capacitance (C^{-1}) was investigated. If the interfacial layer exists at the bottom interface because of the deposition characteristic of our PZT film and the layer is very thin (d ≈ d_{PZT}), the following equation is possible under the series relationship between PZT film and interfacial layer.

$$\frac{1}{C} = \frac{1}{C_i} + \frac{1}{C_{PZT}} \approx \frac{1}{C_i} + \frac{d}{\varepsilon_{PZT}\varepsilon_o A} \qquad (1)$$

where,

C, d, ε = capacitance, thickness, dielectric constant of the total film

C_i, d_i, ε_i = capacitance, thickness, dielectric constant of the interfacial layer

$C_{PZT}, d_{PZT}, \varepsilon_{PZT}$ = capacitance, thickness, dielectric constant of the PZT film

A = area of the electrode

If the film thickness and reciprocal capacitance has a linear relationship, the thickness and property of interfacial layer and the dielectric constant of PZT film are constant regardless of the film thickness. In this study, except the 90 nm thick PZT film, the films well exhibit the linear relationship between d and C^{-1}. In the linear equation obtained from the proper fitting, the dielectric constant of PZT film and the capacitance of interfacial layer (C_i) are represented as the slope of 2556 and the
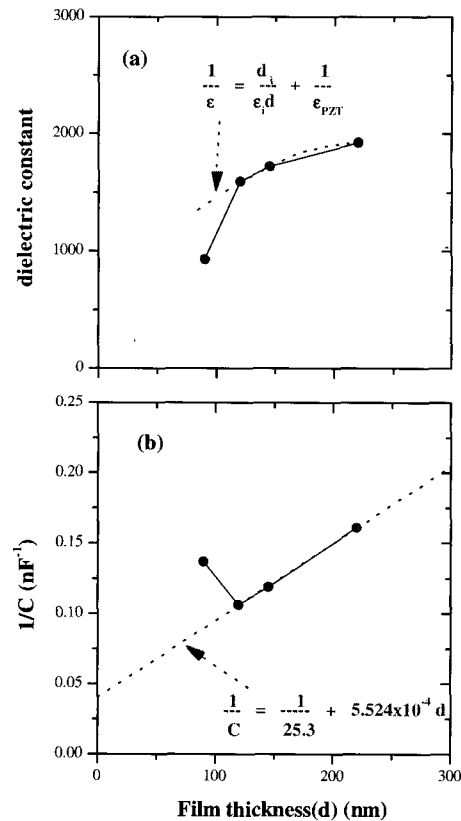

Fig. 1. Dielectric properties of the capacitors with different PZT thickness.

intercept at y-axis of 25.3 nF. The ε_i/d_i value of 35.7 nm^{-1} is derived from C_i = 25.3 nF. If the thickness of interfacial layer is 10 nm, the dielectric constant of the layer is 357. Although there are no significant differences of chemical compositions and XRD patterns between 90 nm thick film and the thicker films, the capacitance characteristic of 90 nm-thick film is degraded, which is attributed to the ferroelectricity degradation of PZT film itself.

Figure 2 shows the variation of the polarization values [switching polarization (P^*), non-switching polarization ($P^\wedge$)] and coercive field (E_C) with increasing the applied electric field (E_a) for the capacitors with different thickness of PZT films. For the PZT films with thickness of above 120 nm, the polarization values and coercive field begin to saturate at the applied fields of above 200 kV/cm. However, for the 90 nm thick film, the polarization value and coercive field do not saturate even at 400 kV/cm. In the virtual ground mode of RT66A ferroelectric tester, P-E hysteresis loops are obtained by integrating the displacement currents with applied electric field. Since this displacement current involves the leakage current of PZT capacitor, the bad leakage current characteristics of PZT capacitors make the P-E hysteresis characteristics not saturate even at the high electric fields. However, in this study, because the 90 nm-thick film shows the good leakage current characteristics as well as the thicker films, it seems that the polarization and P-E hysteresis characteristics with the electric fields are not greatly affected by the leakage
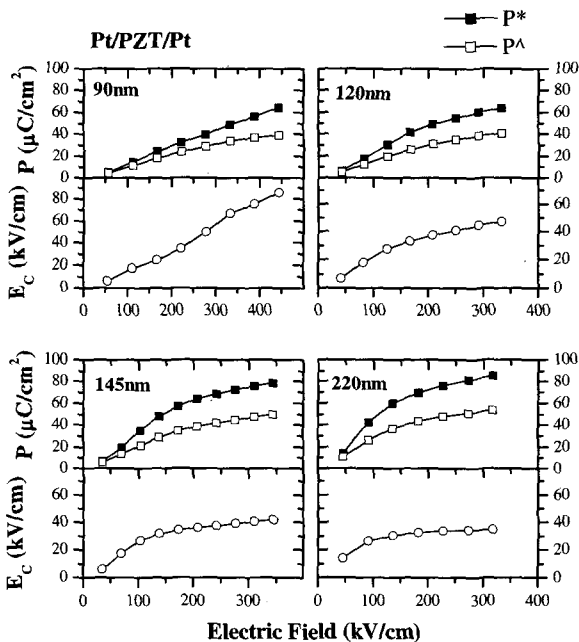
current characteristics. As remarked in above SEM results, the 90 nm thick film has relatively small grains. Since it is relatively difficult to develop the ferroelectric domain structure in such small grains[12], the 90 nm thick film does not exhibit the fully saturated polarization and P-E hysteresis characteristics at the given applied fields.

The polarization fatigue characteristics of PZT capacitors with different film thickness were investigated. Figure 3 shows the variation of polarization values of each PZT capacitor with fatigue cycle at the constant bipolar fields of about 200 kV/cm. The polarization values decrease with fatigue cycles, and the thicker films tend to have a larger initial polarization values and faster degradation rate. In this study, the fatigue cycle at which the $P^*-P^\wedge$ value that is used to discriminate the FRAM logic states drops to 50 % of the initial value is defined as fatigue endurance (N(50 %)). Figure 4 shows the fatigue endurance of PZT capacitors with the film thickness and fatigue pulse height (E_p). The fatigue endurance of 90 nm thick film that does not exhibit the fully saturated polarization characteristic shows a different behavior from the thicker films. The initial polarization values of 90 nm thick film increase and the fatigue endurance of that film decrease with increasing the E_p. However, the initial polarization value and the fatigue endurance of the thicker films are not changed with increasing E_p.

3.2 Fatigue characteristics of the PZT capacitors with different electrode configuration and applied field polarity

Fatigue characteristics of the PZT capacitors were investigated with four different electrode configurations: (top electrode)//(bottom electrode) of Pt//Pt, Pt//RuO_2, RuO_2//Pt, and RuO_2//RuO_2. The PZT films were deposited

Fig. 2. P-E hysteresis characteristics of the capacitors with different PZT thickness.
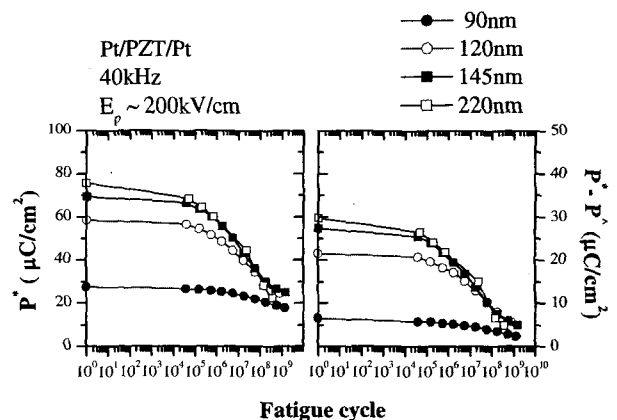

Fig. 3. Polarization fatigue characteristics of the capacitors with different PZT thickness. Fatigue tests were carried out using a bipolar square pulse with 40~50 kHz, 200 kV/cm at room temperature.

on Pt and RuO_2 substrates under the same process conditions. The film thickness, Pb/(Zr+Ti), and Zr/(Zr+Ti) ratios of the PZT film deposited on Pt substrate were 140 nm, 0.98, and 0.47, while those on RuO_2 substrate were 160 nm, 1.11, and 0.45. The deposition characteristics on each substrate were precisely explained in the previous literature[9].

Figure 5 shows the unipolar fatigue characteristics of PZT capacitors with four different electrode configurations. 4 V positive or negative unipolar pulses with a frequency of 50 kHz were applied to top electrodes. In the unipolar fatigue test, the switching polarization (P^*) and non-switching polarization ($P^\wedge$) values were measured by using 2 ms double bipolar pulses at the given cycle. Regardless of the applied field polarity, the unipolar pulses do not cause the polarization fatigue (i.e., the degradation of P^*-$P^\wedge$) of PZT capacitors. In the variation of switching polarization (P^*) with fatigue cycle, the positive unipolar pulse applied to the top electrode decrease the |+P^*| value and increase the |-P^*| value. That is, the positive unipolar pulse can cause the negative polarization-shift, which indicates the negative voltage-shift of P-E hysteresis loop and the existence of downward internal field (from the top electrode to the bottom electrode) in the PZT capacitor. Inversely, the negative unipolar pulse increase the |+P^*| value and decrease the |-P^*| value, which indicates the existence of upward internal field in the PZT capacitor. These results are consistent with other's report on the unipolar fatigue (imprint) for SBT films[4]. All PZT capacitors exhibit the polarization-shifts regardless of their electrode configurations. The directions of polarization-shifts of all PZT capacitors are determined by the applied field polarity.

The development of internal field is attributed to the variation of charge distribution within the PZT capacitor during the unipolar fatigue. If the charged defects in the
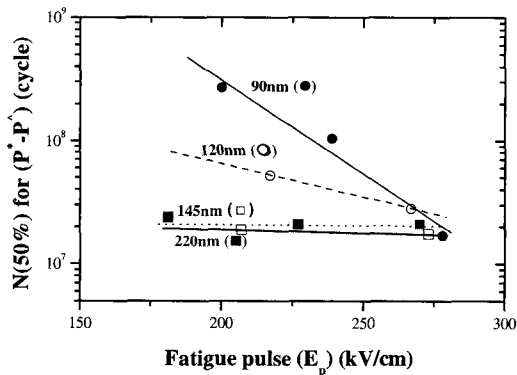
PZT film migrate by the applied filed, the positive unipolar pulse causes the upward internal filed. In this study, however, since the positive unipolar pulse causes the downward internal filed, the negative polarization-shift during the unipolar fatigue is likely to be originated from the charge injection from the electrode, not from the migration of charged defects in the PZT film. That is, during the positive unipolar fatigue, the electrons injected from bottom electrode are trapped at the interface and then form the negative charged state, which results in the downward internal field in the PZT capacitors. Also during the negative unipolar fatigue, it seems that the electrons injected from top electrode result in the upward internal filed. Since the direction of polarization-shifts under the unipolar fatigue is only determined by the applied field polarity regardless of electrode materials and configurations, the charge
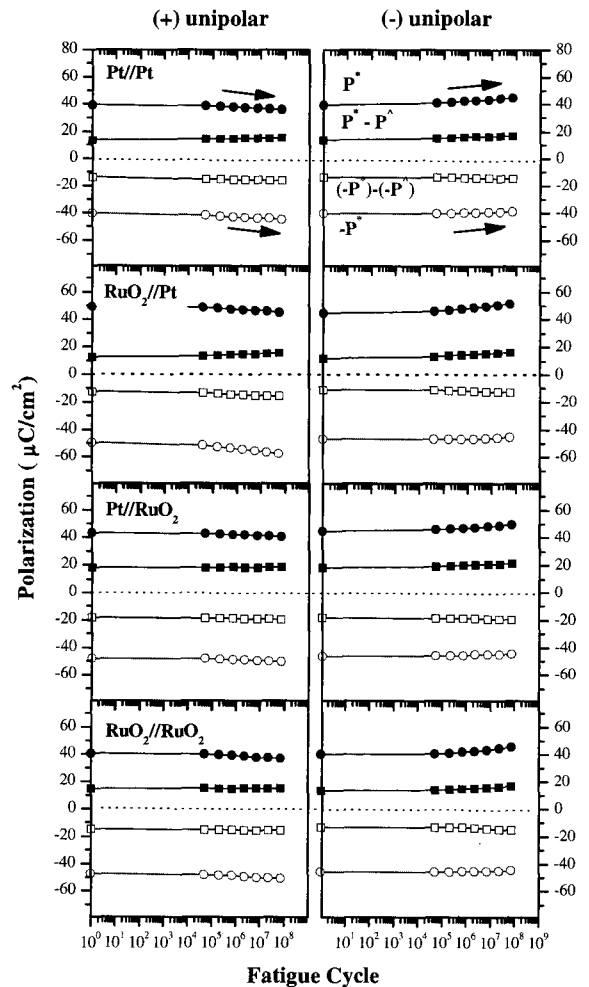

Fig. 5. Unipolar fatigue characteristics of the PZT capacitors with four different electrode configurations. Fatigue tests were carried out using a unipolar square pulse with 50 kHz, 214~250 kV/cm.

Fig. 4. Fatigue endurance [N(50 %)] as a function of the fatigue pulse height for the capacitor with different PZT thickness.

(electron) injections are expected at both top and bottom electrodes regardless of electrode materials.

The temperature dependence of bipolar fatigue characteristics for Pt/PZT/Pt capacitors was investigated. The selected temperatures to investigate the fatigue
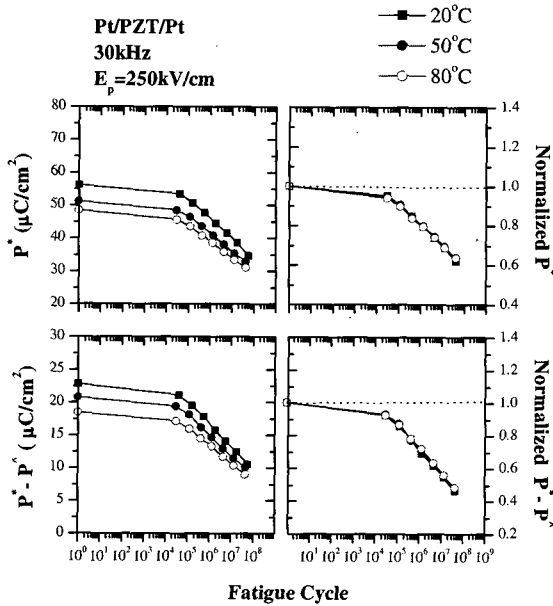

Fig. 6. Temperature dependence of fatigue characteristics of Pt/PZT/Pt capacitors.
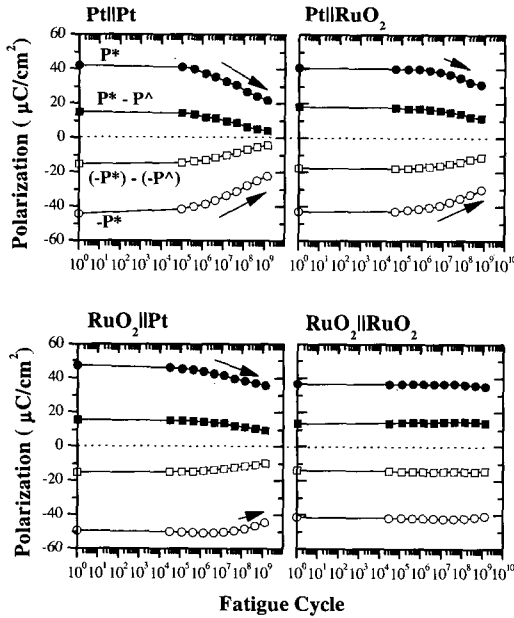

Fig. 7. Bipolar fatigue characteristics of the PZT capacitors with four different electrode configurations. Fatigue tests were carried out using a bipolar square pulse with 30~100 kHz, 188~214 kV/cm at room temperature.

characteristics were 20 °C, 50 °C, and 80 °C and 30 kHz, 250 kV/cm bipolar pulses were applied to the capacitors.

Figure 6 shows that the switching polarization (P^*) and P^*-$P^\wedge$ values decrease with increasing the temperature. In the comparison of normalized values, there are no differences among the fatigue rates at each temperature, which means that the thermal activation energy for the polarization fatigue is nearly zero. This small activation energy indicates that the formation or migration of charged defects already existing in the PZT film or newly formed during the fatigue are unlikely to happen.

Figure 7 shows the bipolar fatigue characteristics of the PZT capacitors with four different electrode configurations. The fatigue tests were carried out by applying bipolar square pulses with 3 V and 30~100 kHz. The Pt//Pt capacitor shows the highest fatigue rate. The capacitors with one Pt electrode (Pt//RuO$_2$ and RuO$_2$//Pt) show lower fatigue rates than the Pt//Pt capacitor. Only the RuO$_2$//RuO$_2$ capacitor remains fatigue-free until the end of the fatigue test (10^{10} cycle). While the negative switching polarization (|-P*|) decreases faster than the positive switching polarization (|+P*|) in the Pt//RuO$_2$ capacitor, the |+P*| decreases faster than |-P*| in the Pt//RuO$_2$ capacitor. The differences of degradation rates between |+P*| and |-P*| (i.e., a kind of polarization-shift) are not observed for the capacitors with symmetric electrode configurations (Pt//Pt and RuO$_2$//RuO$_2$). The polarization-shifts are observed clearly in the capacitors with asymmetric electrode configurations (RuO$_2$//Pt and Pt//RuO$_2$) and the polarization-shifts are in opposite directions. The polarization-shifts of the asymmetric electrode configurations are attributed to the internal field that shifts and/or distorts the P-E hysteresis loop during the fatigue[3].

3.3 Fatigue characteristics of PZT films with domain structure

Ti-oxide seed layers were introduced to control the PZT nucleation conditions so that the PZT films with different domain structure were fabricated on (111)Pt/Ti substrates. Figure 8 shows the XRD patterns and SEM images of the PZT films with and without Ti-oxide seed layer. The PZT film without Ti-oxide seed layer has a {100} preferred orientation and $I_{\{100\}}/I_{\{101\}}$ = 4.25. The chemical composition and grain size of the PZT film with Ti-oxide seed layer with an average thickness of 4nm are nearly the same as those of without Ti-oxide seed layer, but the $I_{\{100\}}/I_{\{101\}}$ ratio greatly decreases to 2.16.

Figure 9 shows the fatigue characteristics of PZT films with different preferred orientations (texture). While the fatigue endurance (N(50 %)) of PZT film with strong {100} texture is about 5×10^7, that with weak {100} texture is above 2×10^8. In this study, since the

PZT film properties such as grain size, chemical composition, and structural phase are not greatly changed with the Ti-oxide seed layer, it is thought that only the texture of PZT film affects the fatigue endurance.

The domain structures of the PZT films with different texture were investigated in the AFM contact mode. Figure 10 shows the AFM topographies and domain images of the PZT films. Since the grain images nearly coincide with the domain images, one grain corresponds to one domain that the dipoles are arranged with a certain direction. In the AFM domain images, the brightest regions represent the 180 ° or −180 ° domains

that dipoles are vertically arranged to the substrate surface, while the darkest regions represent the 90 ° domains. In the AFM domain images, the 90 ° domains of the PZT film with strong {100} texture is much more abundant than that with weak {100} texture. The more 90 ° domains exist in the PZT film, the larger stresses are generated in the PZT film and at the electrode/PZT interface during the domain switching[13], and thus the structural defects may be formed at the vicinity of the electrode/PZT interface. It seems that these structural defects inhibit the domain wall motion and consequently result in the polarization fatigue.

3.4 Fatigue models of CVD-PZT films

In the unipolar fatigue characteristics, the polarization-shifts that the positive pulse decreases the $|+P^*|$ value and increases the $|-P^*|$ value, while the negative

(a) Pt/PZT/Pt

● perovskite
■ Pt substrate

Pb/(Zr+Ti)=1.02
Zr/(Zr+Ti)=0.56
t_{PZT}=145nm

no seed

$I_{(100)}/I_{(101)}$ = 4.247

Pb/(Zr+Ti)=1.01
Zr/(Zr+Ti)=0.55
t_{PZT}=150nm

TiO$_x$ seed

$I_{(100)}/I_{(101)}$ = 2.16

X-ray Intensity (arb. unit)

(100) (001)

(101)

(002) (200)

Si

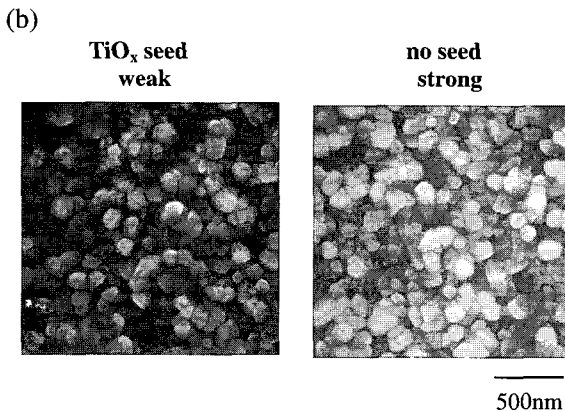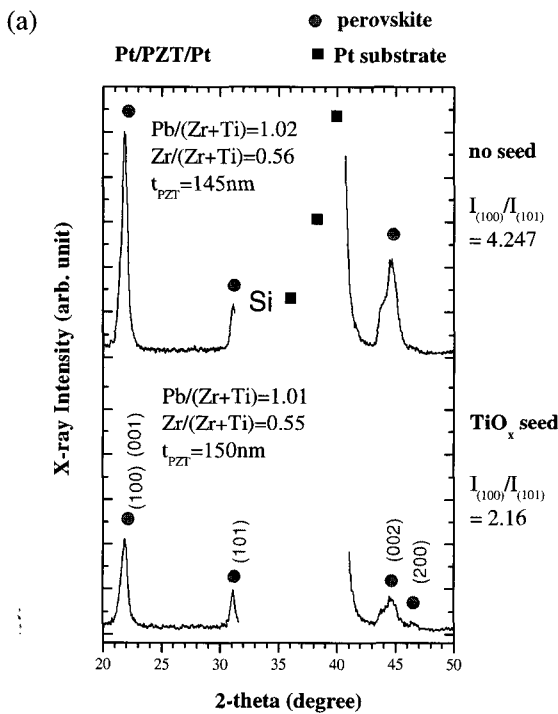2-theta (degree)

(b)

TiO$_x$ seed
weak

no seed
strong

500nm

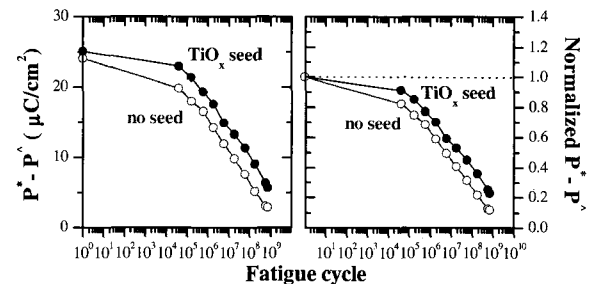Fig. 8. (a) XRD patterns and (b) SEM images of the PZT films on Pt/Ti substrates with and without Ti-oxide seed layer.

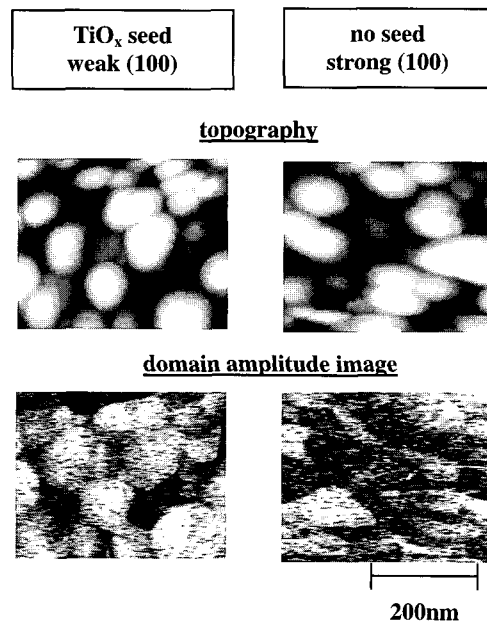Fig. 9. Fatigue characteristics of the PZT films with different textures.

| TiO$_x$ seed weak (100) | no seed strong (100) |

topography

domain amplitude image

200nm

Fig. 10. AFM topographies and domain images of the PZT films with different textures.

pulse increases the |+P*| value and decreases the |-P*| value are observed. The polarization-shifts are attributed to the internal field developed during the unipolar fatigue. In the view of the applied filed polarity and the direction of internal field, the internal field is likely to be originated from charge injections from electrodes, not from the migration of charged defects in PZT film. The charge injections are expected at both Pt and RuO_2 electrodes. However, the unipolar pulse does not degrade the P*-P$^\wedge$ value, which implies that domain switching is necessary for the polarization fatigue.

In the bipolar fatigue characteristics of PZT capacitors with four different electrode configurations, the polarization fatigue occurs in the capacitors where either top or bottom electrode is Pt. And the most severe polarization degradation occurs in the Pt//Pt capacitor. This implies that PZT/Pt interfaces play a decisive role in polarization fatigue. The difference of degradation rates between |+P*| and |-P*| (i.e. the polarization-shifts) in the capacitors with asymmetric electrode configurations suggest the development of internal fields during the fatigue test. The polarization-shifts of PZT capacitors with the asymmetric electrode configurations (Pt/RuO_2, RuO_2//Pt) are in opposite directions, which mean that the electrode configurations determine the direction of the internal fields. The internal fields are attributed to the difference of charged defect densities between top and bottom interfaces during the fatigue. In this study, there is no temperature dependence of fatigue rates of PZT capacitors. Additionally, in the unipolar fatigue characteristics, the migration of charged defects by the applied field is not expected in the PZT film. Therefore, the development of internal fields during the fatigue is not attributed to the migration of charged defects in PZT film, but to the difference of charged defect densities between top and bottom interfaces during the domain switching. However, since the Pt/PZT interface plays a decisive role to the fatigue and the electrode configurations of Pt and RuO_2 determine the direction of internal fields, the charged defect density at the Pt/PZT interface is much higher than that at the RuO_2/Pt interface. It is thought that this charged defect is oxygen vacancy ($V_O^{\bullet\bullet}$) and it may be generated by the stress during the domain switching. Because RuO_2 electrode has tolerance for oxygen vacancy to a certain degree, the oxygen vacancies generated during the fatigue are easily removed at the RuO_2/PZT interface. The charged defects contribute to the domain wall pinning and degrade the polarization of PZT film. Consequently, the PZT film at the vicinity of Pt electrode exhibit the fatigue, and when the top and bottom electrode configurations are of asymmetric (Pt//RuO_2, RuO_2//Pt), the difference of charged defect densities between top and bottom interfaces causes the internal field and the resultant polarization-shift.

4. CONCLUSION

Fatigue characteristics of CVD-PZT films were investigated with the film properties (thickness, domain structure) and the measuring conditions (unipolar, bipolar, temperature). In the fatigue characteristics with PZT film thickness and fatigue pulse height, the fatigue rates are independent of the fatigue pulse height at the electric field regions to saturate the P-E hysteresis and polarization (P*, P$^\wedge$) characteristics. But the fatigue rates are varied with fatigue pulse height at the field regions not to saturate the characteristics. In the unipolar fatigue characteristics of PZT capacitors with four different electrode configurations (Pt//Pt, Pt//RuO_2, RuO_2//Pt, and RuO_2//RuO_2), the polarization-shifts are attribute to the charge injection from electrodes, not to the migration of charged-defects in the PZT films. The difficulty of the charged defect migration is also shown in the results of temperature dependence of fatigue rates. Since the polarization degradations do not occur with the unipolar pulse, it seems that the polarization fatigue occurred during the domain switching. The charged defects may be generated during the domain switching particularly at the electrode/PZT interfaces and those are accumulated only at the Pt/PZT interface while not at the RuO_2/PZT interface. This suggests that the charged defects should be oxygen vacancy ($V^{\bullet\bullet}$). And thus the PZT capacitors where either top or bottom electrode is Pt, show distinct polarization fatigues. The Pt//RuO_2 and RuO_2//Pt capacitors with asymmetric electrode configurations exhibit the polarization-shifts during fatigue due to the difference of charged defect densities between Pt/PZT interface and RuO_2/PZT interface. The PZT film with large amount of non-180 $^\circ$ domains exhibits the fast fatigue rate by the large stress generated during the domain switching.

ACKNOWLEDGMENTS

REFERENCES

[1] H. M. Duiker, P. D. Beale, J. F. Scott, C. A. Paz de Araujo, B. M. Melnick, J. D. Cuchioaro, and L. D. McMillan, "Fatigue and switching in ferroelectric memories: Theory and experiment", J. Appl. Phys, Vol. 68, No. 11, p. 5783, 1990.

[2] W. L. Warren, D. Dimos, B. A. Tuttle, R. D. Nasby, and G. E. Pike, "Electronic domain pinning in Pb(Zr,Ti)O$_3$ thin films and its role in fatigue", Appl.

Phys. lett., Vol. 65, No. 8, p. 1018, 1994.

[3] X. Du and I. W. Chen, "Fatigue of $Pb(Zr_{0.53}Ti_{0.47})O_3$ ferroelectric thin films", J. Appl. Phys., Vol. 83, No. 12, p. 7789, 1998.

[4] T. Hase, T. Noguchi, K. Takenura, and Y. Miyasaka, "Imprint characteristics of $SrBi_2Ta_2O_9$ thin films with modified Sr composition", Jpn. J. Appl. Phys., Vol. 37, No. 9B, p. 5198, 1998.

[5] D. Ricinschi and M. Okuyama, "Relationships between macroscopic polarization hysteresis and local piezoresponse of fatigued $Pb(Zr,Ti)O_3$ films within a Landau theory-based lattice model", Appl. Phys. Lett., Vol. 81, No. 21, p. 4040, 2002.

[6] A. Jiang, M. Dawber, J. F. Scott, C. Wang, P. Migliorato, and M. Gregg, "Studies of switching kinetics in ferroelectric thin films", Jpn. J. Appl. Phys., Vol. 42, No. 11, p. 6973, 2003.

[7] B. S. Kawk, E. P. Boyd, and A. Erbil, "Metalorganic chemical vapor deposition of $PbTiO_3$ thin films", Appl. Phys. Lett., Vol. 53, No. 18, p. 1702, 1988.

[8] S. O. Chung, J. W. Kim, S. T. Kim, G. H. Kim, and W. J. Lee, "Microstructure and electric properties of the PZT thin films fabricated by ECR PECVD: the effects of an interfacial layer and rapid thermal annealing", Mat. Chem. & Phys., Vol. 53, No. 1, p. 60, 1998.

[9] S. O. Chung, H. C. Lee, and W. J. Lee, "Effects of electrodes on the electric properties of $Pb(Zr,Ti)O_3$ films deposited by electron cyclotron resonance plasma enhanced chemical vapor deposition", Jpn. J. Appl. Phys., Vol. 39, No. 3A, p. 1203, 2000.

[10] K. M. Byun, J. W. Kim, and W. J. Lee, "Theoretical composition calibration and thickness measurement in the analysis of multielement thin films using wavelength dispersive spectroscopy: applications to lead zirconate titanate thin films", Jpn. J. Appl. Phys., Vol. 36, No. 9AB, p. L1242, 1997.

[11] S. O. Chung, J. W. Kim, G. H. Kim, C. O. Park, and W. J. Lee, "Formation of a lead zirconate titanate (PZT)/Pt interfacial layer and structural changes in the $Pt/Ti/SiO_2/Si$ substrate during the deposition of PZT thin film by electron cyclotron resonance plasma-enhanced chemical vapor deposition", Jpn. J. Appl. Phys., Vol. 36, No. 7A, p. 4386, 1997.

[12] H, Funakubo, T. Hioki, M. Otsu, K. Shinizaki, and N. Mizutani, "Film thickness dependence of dielectric property and crystal structure of $PbTiO_3$ film prepared on $Pt/SiO_2/Si$ substrate by metal organic chemical vapor deposition", Jpn. J. Appl. Phys., Vol. 32, No. 9B, p. 4175, 1993.

[13] T. Tsurumi, Y. Kumano, N. Ohashi, T. Takenaka, and O. Fukunaga, "90 ° domain reorientation and electric-field-induced strain of tetragonal lead zirconate titanate ceramics", Jpn. J. Appl. Phys., Vol. 36, No. 9B, p. 5970, 1997.